Cluster Ion Thermal Decomposition (I): Experimental Kinetics Study and ab Initio Calculations for $HSO_4^-(H_2SO_4)_x(HNO_3)_y$

Joachim Curtius,[†] Karl D. Froyd,[†,‡] and Edward R. Lovejoy*

NOAA Aeronomy Laboratory, 325 Broadway, Boulder, Colorado 80305

Received: July 2, 2001; In Final Form: September 26, 2001

Rate coefficients for the thermal decomposition of cluster ions of the type $HSO_4^-(H_2SO_4)_x$ for $x = 1-5$, $HSO_4^-(HNO_3)_y$ for $y = 1, 2$ and $HSO_4^-H_2SO_4HNO_3$ were measured as functions of temperature and pressure in a quadrupole ion trap. The measured decomposition kinetics are in the low-pressure limit or in the fall-off region between the low and high-pressure limits. Moments of inertia and vibrational frequencies of the clusters were obtained via ab initio HF/6-31+G(d) geometry optimizations. Bond energies were determined from analysis of the second-order rate coefficient data for the cluster ions with kinetics in the low-pressure limit. Upper limits of the bond energies were derived for the clusters with kinetics in the fall-off region.

Introduction

Ions containing sulfuric acid and nitric acid are the most abundant negative ions in the stratosphere and the free troposphere.[1] Recently, the formation of aerosol particles by ion-induced nucleation has received renewed attention as an important source of atmospheric aerosol.[2] Sulfuric acid is thought to play a significant role in this nucleation process. Ion-induced nucleation of sulfuric acid, water, and organic molecules is also thought to take place in the wake of jet aircraft.[3] Nevertheless, the mechanism of ion-induced nucleation in the atmosphere as well as in jet aircraft exhaust is poorly understood and only limited thermochemical and kinetic data for the elementary clustering reactions exist.[4] Attempts to model the measured atmospheric nucleation events using classical nucleation theory have been only partially successful.[5] This is not surprising because input parameters of classical nucleation theory involve bulk properties of the nucleating substances (density and surface tension) which are most probably not applicable to molecular clusters that consist only of a few molecules.

Here, experimental kinetic measurements and ab initio calculations which provide thermochemical information about the first association steps of H_2SO_4 and HNO_3 molecules to the HSO_4^- core ion are presented. Rate coefficients k_d of the dissociation reactions of cluster ions are derived from the measurements. Vibrational frequencies ν, average vibrational energies U_{vib}, moments of inertia I and entropies S of the different clusters are calculated ab initio from the optimized molecular structures. The bond energies for cluster ions with kinetics in the low-pressure limit are calculated from these quantities based on a procedure developed previously for cluster ions in the low-pressure limit.[6,7] The analysis also yields upper limits of the bond energies for cluster kinetics in the fall-off regime ($HSO_4^-(H_2SO_4)_x$, ($x = 2-5$)). The thermochemical properties of the cluster ions investigated here have not been determined previously in the laboratory. However, Arnold and co-workers reported thermochemical data for most of the cluster ions presented here based on stratospheric measurements of ion distributions.[8]

The accompanying paper by Lovejoy and Curtius, hereafter termed paper (II),[27] presents the development and application of a master equation model that is used to derive the bond energies for cluster ions in the fall-off region from the present measurements and ab initio results.

The bond energies E_0 coupled with the vibrational frequencies, the moments of inertia, and the entropies yield the free energies ΔG for molecular association/dissociation steps that are needed for the modeling of ion-induced aerosol nucleation.

Experimental Details

The ion trap apparatus used in the present work is similar to the one described previously.[7,9] A new ion trap with an internal radius of 1 cm, modified hyperbolic angle geometry[10] and electrodes that extend to a 3 cm radius was employed. The performance of the new trap is comparable to the former trap with the advantages of less statistical variation in the ion signals and better resolution at large mass numbers (>500 amu). The new trap is temperature controlled in a range between 30 °C and 340 °C. Heaters, similar to the ones described in detail by Lovejoy and Bianco,[7] were installed. The new heaters allow a uniform heating of the ion trap. At steady state, the ring electrode is slightly colder than the two end caps, about 1 °C at 30 °C to about 12 °C at 340 °C average temperature. Because the helium buffer gas has many collisions with the end caps and the ring electrode during its residence time in the trap, it is assumed that the temperature of the He bath gas is the average of the end cap and the ring electrode temperatures. It has been demonstrated that the internal temperature of the ions is very close to the bath gas temperature.[7,11] During the measurements, the average temperature of the ion trap is constant to within ±1 °C.

Ions were produced by a filament electron source in a flow reactor with helium as the carrier gas. Gaseous sulfuric acid was added to the flow reactor downstream of the ion source by passing helium over liquid sulfuric acid at ~70 °C. Gaseous sulfuric acid reacted with charged particles from the filament

* To whom correspondence should be addressed. E-mail: Edward.R.Lovejoy@al.noaa.gov.

[†] Also affiliated with Cooperative Institute for Research in Environmental Sciences, University of Colorado, Boulder, Colorado.

[‡] Also affiliated with Department of Chemistry and Biochemistry, University of Colorado, Boulder, Colorado.

10.1021/jp0124950 CCC: $20.00
Published on Web 11/08/2001

source, leading to cluster ions of the type $HSO_4^-(H_2SO_4)_x$. Gaseous nitric acid was added to the flow reactor by bubbling helium gas through a reservoir of concentrated HNO_3. The composition of the cluster ions was controlled by adjusting the flows of helium over the sulfuric and nitric acid and by adjusting the pressure in the flow reactor (typically 5 Torr). A small portion of the reactor flow entered the ion trap chamber through a 0.25 mm orifice. Ion clusters were extracted from the sampled gas and focused into the ion trap by use of electrostatic lenses. A critical orifice ($d = 5.1$ mm) located between the flow reactor and the entrance orifice of the mass spectrometer allows the flow reactor to be operated at even higher pressures (up to 15 Torr) without significantly increasing the flow into the ion trap chamber. The pressure in the differential pumping stage between flow reactor and ion trap entrance orifice was <0.1 Torr. The higher pressure and the longer residence time in the flow reactor as well as the adiabatic expansion downstream of the critical orifice enhanced the formation of the large ion clusters.

Computational Details

The ab initio calculations were performed at the HF/6-31+G(d) level of theory. Diffuse *s* and *p* shells were added to the second and third row atoms in order to improve the representation of the anion proton affinities.[12] The purpose of the calculations was to determine the vibrational frequencies and the moments of inertia of the optimized molecular structures. Corrections for basis set superposition error[12,13] and electron correlation energies[12,14,15] were not performed. Vibrational frequencies were scaled by 0.89 for the calculation of thermochemical properties.[7,16] All quantum chemical ab initio calculations were performed using the GAMESS software package[17] and the output was visualized with the MOLDEN software.[18] The geometry optimizations were performed with a maximum energy gradient tolerance of 1×10^{-5} hartree bohr^{-1} or better.

Experimental Section

The kinetics of thermal decomposition of the $HSO_4^-(H_2SO_4)_x(HNO_3)_y$ ions were studied by monitoring the variation of the cluster ion signal as a function of the ion trap residence time. The experimental procedures were similar to those described previously.[7] The temporal evolution of the $HSO_4^-(H_2SO_4)_4$ cluster ions (489 amu) in the trap at 314 K is displayed in Figure 1(a−c). The ion cluster was isolated using a filtered noise field during the trapping period. The mass spectra were recorded after shutting off the filter and trapping the ions for reaction times of 10 ms (a), 100 ms (b), and 500 ms (c). The dissociation reactions

$$HSO_4^-(H_2SO_4)_4 \rightarrow HSO_4^-(H_2SO_4)_3 + H_2SO_4 \qquad (1)$$

and

$$HSO_4^-(H_2SO_4)_3 \rightarrow HSO_4^-(H_2SO_4)_2 + H_2SO_4 \qquad (2)$$

are observed.

Examples of ion signals (integrated peak area) as a function of reaction time for the decay of $HSO_4^-(H_2SO_4)_4$ are presented in Figure 2. The decay of the reactant ($HSO_4^-(H_2SO_4)_4$) and the build-up of the product ion ($HSO_4^-(H_2SO_4)_3$) are shown (reaction (1)), as well as the increase of the next smaller cluster ($HSO_4^-(H_2SO_4)_2$) in the subsequent decomposition reaction (2). A small amount of $HSO_4^-(H_2SO_4)_5$ remained in the trap despite the filtering, but the signal was <1% of the $HSO_4^-(H_2SO_4)_4$ signal and decayed rapidly. The data were fit by an exponential decay function weighted by the reciprocal of the signal to derive the pseudo-first-order rate coefficient (k_d^I). This weighting is appropriate for the statistics of counting experiments which are represented by a Poisson distribution ($\sigma^2 = N$; N = number of counts). The variation of the pseudo-first-order rate coefficients as a function of Helium pressure in the trap for several temperatures is shown in Figure 3. The coefficients for the decay of $HSO_4^-(H_2SO_4)_4$ over the full accessible pressure range for two temperatures are displayed in Figure 3(a). The data are curved, suggesting that the kinetics are in the fall-off regime, and a simple linear determination of k_d^{II}, the second-order decomposition rate coefficient, gives a lower limit to the low-pressure limit rate constant $k_d^{II}{}_{lpl}$. A more sophisticated analysis

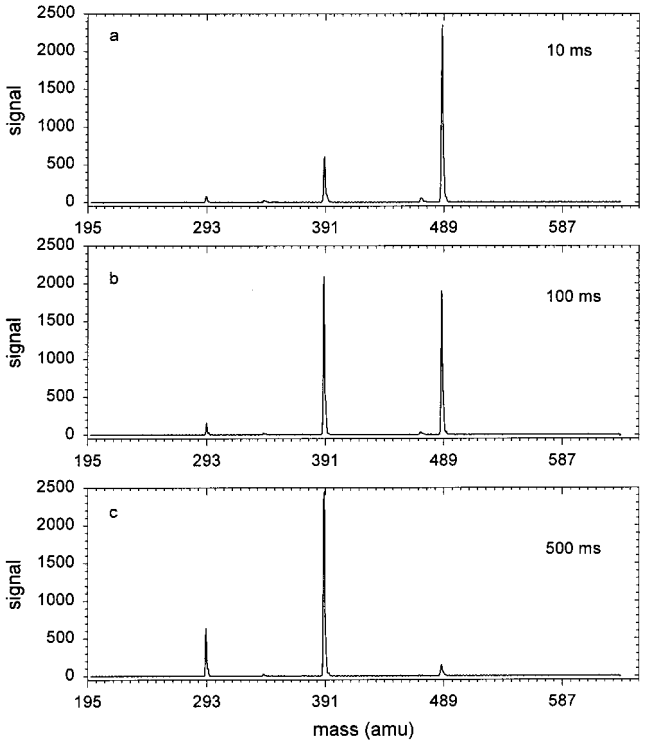

Figure 1. Mass spectra of $HSO_4^-(H_2SO_4)_4$ decomposition (mass: 489 amu) as measured in the ion trap at three different reaction times: 10 ms (a), 100 ms (b), and 500 ms (c). Ion trap parameters: Axial modulation = 100 kHz, $q_z = 0.13$, trapping time = 25 ms, $T = 314$ K, $p_{He} = 0.3$ mTorr, 10 spectra averaged.

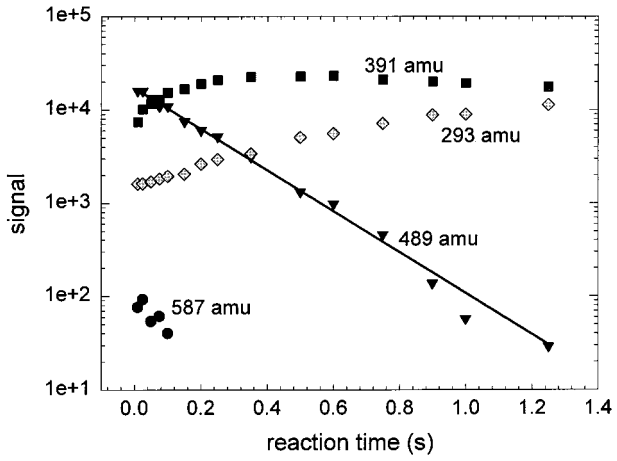

Figure 2. Mass spectrometric signals for the unimolecular decomposition of $HSO_4^-(H_2SO_4)_4$ (m = 489 amu) and its product ions at T = 314 K and $p = 0.30$ mTorr as a function of reaction time. First-order rate coefficients k_d^I are derived from the slope of the $HSO_4^-(H_2SO_4)_4$ signal.

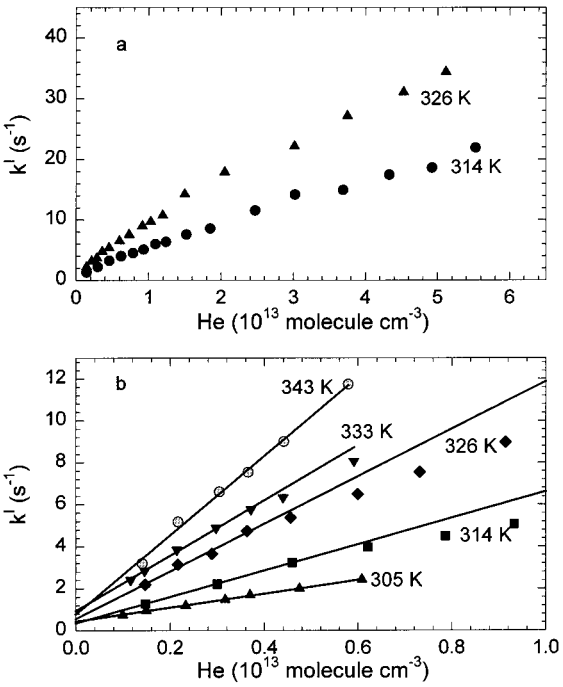

Figure 3. First-order decomposition rate coefficients k_d^I as a function of Helium pressure in the ion trap at several temperatures for $HSO_4^-(H_2SO_4)_4$ for the full pressure range (a), and for the lowest accessible pressure range (b). Lines are linear fits to the data for [He] $< 6 \times 10^{12}$ molecule cm^{-3}.

of these data shows that it is possible to derive rate coefficients and bond energies when full master equation modeling is performed (see paper (II)). Additional measurements were made at the lowest pressures accessible (Helium buffer gas concentration: $1-6 \times 10^{12}$ molecule cm^{-3}). Illustrative results are shown in Figure 3(b). In this pressure range, the data can be fitted by straight lines, however, slight curvature can already be observed for the $HSO_4^-(H_2SO_4)_4$ cluster at helium concentrations around 5×10^{12} molecule cm^{-3}. Additionally, intercepts that increase with increasing temperature are observed. As shown in paper (II) these intercepts are not caused by additional loss processes, but indicate that the kinetics are not in the low-pressure range. The k_d^{II} values derived for the $HSO_4^-(H_2SO_4)_x$ ($x = 2-5$) cluster decomposition reactions are therefore just lower limits to the low-pressure limit rate coefficients. The second-order rate coefficients are plotted as a function of temperature for all clusters studied as an Arrhenius plot in Figure 4. For all cluster decomposition reactions in which a significant curvature at higher pressures is observed ($HSO_4^-(H_2SO_4)_x$, $x = 2-5$), the second order coefficients were determined by fitting the data only in the lowest pressure region ([He] $< 6 \times 10^{12}$ molecule cm^{-3}).

Ab Initio Studies

The ab initio calculations give insight into the molecular structures, and yield the moments of inertia and vibrational frequencies of the ion clusters. These quantities are inputs for the master equation calculations discussed in paper (II) and were used for calculating thermochemical parameters of the unimolecular reactions studied. Several of the optimized structures of the molecules and clusters are shown in Figure 5. The HSO_4^- ion 5(a), the H_2SO_4 molecule 5(b), the $HSO_4^-H_2SO_4$ cluster 5(c), HNO_3 5(d), HSO_4^- with one and two HNO_3 ligands 5(e, f) and two configurations of the mixed cluster $HSO_4^-H_2SO_4$-HNO_3 5(g, h) are shown. Optimized structures of the $HSO_4^-(H_2SO_4)_x$, $x = 1-5$, complexes and their corresponding thermodynamic quantities will be published elsewhere (R. Bianco, to be submitted).

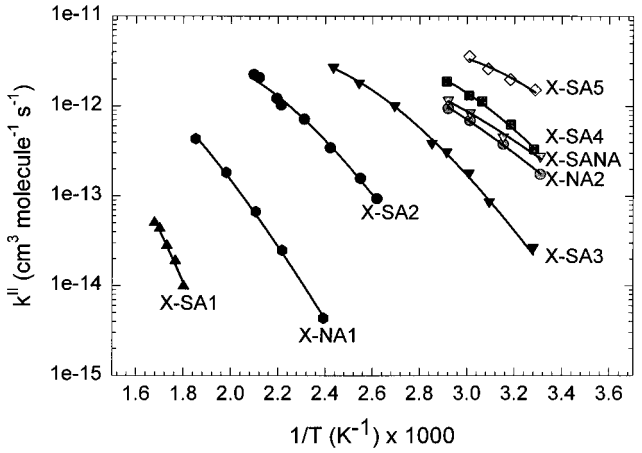

Figure 4. Temperature dependence of the measured second-order rate coefficients in Arrhenius form (symbols). The solid lines are fits to eq 5 that yield bond and activation energies. The acronyms $X^- = HSO_4^-$, SA $= H_2SO_4$, and NA $= HNO_3$ are used.

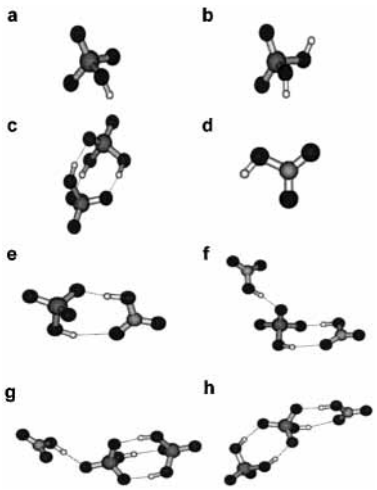

Figure 5. Molecular structures of cluster ions and ligand molecules: (a) HSO4$^-$; (b) H_2SO_4; (c) $HSO_4^-H_2SO_4$; (d) HNO_3; (e) $HSO_4^-HNO_3$; (f) $HSO_4^-(HNO_3)_2$; (g) $HSO_4^-H_2SO_4HNO_3$; and (h) $HSO_4^-H_2SO_4HNO_3$ alternate structure.

The C_2 configuration of sulfuric acid displayed in Figure 5(b) is the energetically most stable configuration[19,20] of H_2SO_4. The $HSO_4^-H_2SO_4$ cluster in which the ligand is bonded to the core ion by three hydrogen bonds is shown in Figure 5(c). The exceptionally high bond energy of this cluster originates from this strong triple bond as shown previously by Evleth.[21]

Two isomers of the $HSO_4^-(H_2SO_4)_2$ cluster were optimized. One of the structures, hereafter termed 2α, maintains the underlying triple H-bond structure of the $HSO_4^-H_2SO_4$ entity. Structure 2β contains the same number of hydrogen bonds as the 2α structure, but instead of the triply bonded $HSO_4^-H_2SO_4$ core, an H-bond between the two H_2SO_4 ligand molecules is established (R. Bianco, to be submitted). The total energies of the respective clusters were found to be very similar (within 1 kcal mol^{-1}). Here, the total energy denotes the sum of the electronic and zero point energy of the HF/6-31+G(d) optimizations.

Two alternate structures of the $HSO_4^-(H_2SO_4)_3$ cluster were optimized (3α and 3β). Similar to the $HSO_4^-(H_2SO_4)_2$ cluster, the triply bonded $HSO_4^-H_2SO_4$ structure is maintained in 3α,

TABLE 1: Electronic Energies E_{el}, Zero Point Energies E_{ZP}, Average Vibrational Energies U_{vib} (at 298 K), Geometric Mean of the Moments of Inertia I_{gm} and Entropies $S°$ (at 298 K) Obtained from ab Initio Calculations

species	E_{el} (hartrees)	E_{ZP} (kcal mol^{-1})	U_{vib}(298.15 K) (kcal mol^{-1})	$I_{geom.mean}$ (amu nm^2)	$S°_{298.15}$ (cal mol^{-1} K^{-1})
H_2SO_4	−698.048 76	23.7	1.5	1.0	72.5
HNO_3	−279.453 70	16.6	0.4	0.5	63.3
HSO_4^-	−697.546 07	16.5	1.3	1.0	71.9
$HSO_4^-H_2SO_4$	−1395.663 02	42.4	4.6	5.3	100.4
$HSO_4^-(H_2SO_4)_2^{a:2\alpha}$	−2093.757 21	67.7	8.6	15.7	137.1
$HSO_4^-(H_2SO_4)_2^{a:2\beta}$	−2093.755 65	67.6	8.5	14.6	134.7
$HSO_4^-(H_2SO_4)_3^{a:3\alpha}$	−2791.838 83	92.7	12.9	33.1	175.8
$HSO_4^-(H_2SO_4)_3^{a:3\beta}$	−2791.841 77	92.8	12.7	30.6	172.9
$HSO_4^-(H_2SO_4)_4$	−3489.926 98	117.9	16.7	48.6	208.2
$HSO_4^-(H_2SO_4)_5$		142.8[b]	20.7[b]	73.1[b]	244.5[b]
$HSO_4^-HNO_3$	−977.043 23	34.0	4.1	4.2	99.4
$HSO_4^-(HNO_3)_2$	−1256.530 73	51.5	7.4	12.4	136.2
$HSO_4^-H_2SO_4HNO_3^{a:5(g)}$	−1675.147 30	59.8	7.9	13.4	138.6
$HSO_4^-H_2SO_4HNO_3^{a:5(h)}$	−1675.143 61	59.6	8.1	13.3	136.2

[a] Alternative structures (cf. text). [b] Extrapolated.

whereas an interligand H-bond is established in 3β. Again, both structures are similar in total energy (within 2 kcal/mol). The $HSO_4^-(H_2SO_4)_4$ cluster is a structure without the triply bonded $HSO_4^-H_2SO_4$ entity but with three inter-ligand H-bonds. No alternate structures were calculated for this cluster due to computational restraints. An in-depth discussion of the $HSO_4^-(H_2SO_4)_x$, $x = 1-5$, geometries will be given by R. Bianco (to be submitted).

The planar structure of the HNO_3 molecule is depicted in Figure 5(d). The optimized geometry of the $HSO_4^-HNO_3$ cluster is given in 5(e), and in 5(f) the $HSO_4^-(HNO_3)_2$ structure is shown. Figures 5(g) and 5(h) show two structures of the mixed $HSO_4^-H_2SO_4HNO_3$ cluster. The energy of the structure based on the triply bonded $HSO_4^-H_2SO_4$ (Figure 5(g)) is predicted to be 2.1 kcal mol^{-1} lower than that of the structure shown in Figure 5(h).

The results from the ab initio studies are summarized in Table 1. Electronic energies, zero point energies, vibrational energies, standard entropies, and the geometric mean of the moments of inertia are presented. The electronic energies of HSO_4^-, H_2SO_4 and $HSO_4^-H_2SO_4$ agree with Evleth's HF/6-31+G(d) results within 0.02 kcal mol^{-1}.[21] Due to computational limitations, the vibrational frequencies of the $HSO_4^-(H_2SO_4)_5$ cluster were derived from an extrapolation of the frequencies of $HSO_4^-(H_2SO_4)_4$. A set of frequencies consistent with adding another H_2SO_4 ligand, based on the differences between the $HSO_4^-(H_2SO_4)_3$ (3β structure) and the $HSO_4^-(H_2SO_4)_4$ cluster, was appended to the $HSO_4^-(H_2SO_4)_4$ frequency set. Similarly, the geometric mean moment of inertia and the standard entropy of $HSO_4^-(H_2SO_4)_5$ were also extrapolated based on the trends in the smaller clusters.

The distribution of vibrational frequencies for H_2SO_4 and the $HSO_4^-(H_2SO_4)_x$ clusters are shown in Figure 6. The intramolecular frequencies of liquid sulfuric acid are also shown for comparison (from reference 22). Going from smaller to larger clusters, the discrete frequencies evolve into groups of frequencies, e.g., the single OH-stretch vibration of HSO_4^- at 3642 cm^{-1} (or the O−H stretches of H_2SO_4 at 3584 and 3588 cm^{-1}) transforms into a set of O−H stretch vibrations between 3200 and 3400 cm^{-1}. The frequencies are red-shifted by about 300 cm^{-1} due to the intermolecular deceleration of the vibration by the H-bonds, whereas the frequencies of liquid H_2SO_4 are shifted by more than 600 cm^{-1}. A similar effect has been calculated for sulfuric acid O−H stretch vibrations when H_2SO_4 is hydrated[20] or ammoniated[23] and for the O−H stretch of water clusters.[24] Another example is the evolution of the two normal

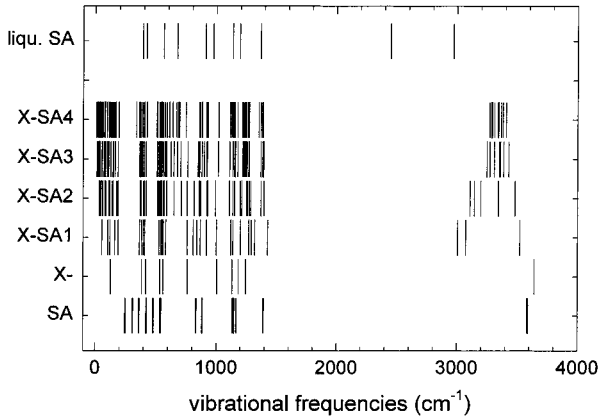

Figure 6. Calculated vibrational frequencies for H_2SO_4 and $HSO_4^-(H_2SO_4)_x$ ($x = 0-4$; for $x = 2$, 3 the frequencies of the more stable isomers (2α and 3β) are shown) and liquid sulfuric acid (from ref 22). Acronyms are as described in the caption of Figure 4.

modes of the O−S−O bends of HSO_4^- at 383 and 419 cm^{-1} into a band around 400 cm^{-1}. All frequencies were calculated in the harmonic oscillator approximation.

Thermochemical parameters of the clusters as listed in Table 1 are displayed in Figure 7. The increase of the average vibrational energy at 298.15 K is shown in Figure 7(a). A regression using the $HSO_4^-(H_2SO_4)_x$ data for $x = 1-4$ shows the linear dependence of vibrational energy with increasing cluster size. The $HSO_4^-(H_2SO_4)_5$ cluster's vibrational energy, calculated using the augmented frequency set, lays also on the straight regression line.

The geometric mean of the moments of inertia I_{gm} of the clusters is displayed in Figure 7(b). For all clusters studied, I_{gm} increases monotonically as the number of ligands increases. To extrapolate I_{gm} for the $HSO_4^-(H_2SO_4)_5$ cluster a quadratic function was fitted to the $HSO_4^-(H_2SO_4)_x$ ($x = 0-4$) data.

The entropies of the different clusters increase as a function of the number of ligands (Figure 7(c)) and for both, H_2SO_4 and HNO_3, a linear regression from the sulfuric acid clusters ($x = 1-4$) describes the relation well. The entropy of the $HSO_4^-(H_2SO_4)_5$ cluster was extrapolated from a linear fit to the $HSO_4^-(H_2SO_4)_x$ ($x = 1-4$) data. For $x > 1$ each additional H_2SO_4 ligand adds about 36.2 entropy units to the cluster. Considering the calculated entropy value of 72.5 cal mol^{-1} K^{-1} for gaseous H_2SO_4 (Table 1), the entropy change for the reaction $HSO_4^-(H_2SO_4)_x \rightarrow HSO_4^-(H_2SO_4)_{x-1} + H_2SO_4$ is approximately $\Delta S \approx 36.3$ cal mol^{-1} K^{-1} for clusters with $2 \leq x \leq 5$.

TABLE 2: Bond Energies and Activation Energies Derived from Fitting the Experimental Data

reaction	q_z[a]	T_{avg} (K)	E_0 (kcal mol^{-1})	U_{vib} (T_{avg}) (kcal mol^{-1})	E_a (T_{avg}) (kcal mol^{-1})	$E_{0,a.i.}$ (kcal mol^{-1})	$\Delta S°_{298.15}$ (cal mol^{-1} K)
$HSO_4^-H_2SO_4 \rightarrow HSO_4^- + H_2SO_4$	0.23	576.4	43.3	15.5	26.5	40.6	44.0
$HSO_4^-(H_2SO_4)_2 \rightarrow HSO_4^-H_2SO_4 + H_2SO_4$	0.17	434.4	<28.7	16.8[b]	10.8	26.9	35.8[b]
$HSO_4^-(H_2SO_4)_3 \rightarrow HSO_4^-(H_2SO_4)_2 + H_2SO_4$	0.14	348.3	<28.8	16.6[b]	11.3	21.2	36.7[b]
$HSO_4^-(H_2SO_4)_4 \rightarrow HSO_4^-(H_2SO_4)_3 + H_2SO_4$	0.13	324.1	<29.1	19.3	9.0	21.7	37.1
$HSO_4^-(H_2SO_4)_5 \rightarrow HSO_4^-(H_2SO_4)_4 + H_2SO_4$	0.10	318.5	<29.7	23.2[c]	5.8		36.2[c]
$HSO_4^-HNO_3 \rightarrow HSO_4^- + HNO_3$	0.10	478.0	27.2	9.4	16.7	26.4	35.8
$HSO_4^-(HNO_3)_2 \rightarrow HSO_4^-HNO_3 + HNO_3$	0.18	323.4	17.7	8.4	8.5	20.3	26.5
$HSO_4^-H_2SO_4HNO_3 \rightarrow HSO_4^-H_2SO_4 + HNO_3$	0.16	323.4	17.3	9.1[b]	7.4	18.5	25.0[b]

[a] Trapping parameter q_z as defined in ref 7. [b] Vibrational frequencies of the most stable isomers 2α, 3β and the structure shown in Figure 5(g) used for calculation of U_{vib} and $\Delta S°_{298.15}$ (cf. text and Figure 5). [c] Extrapolated.

This is already close to the H_2SO_4 vaporization entropy (35.0 cal mol^{-1} K^{-1}, bulk solution standard entropy[22]).

Discussion

The Arrhenius activation energy is defined as

$$E_a = \frac{\partial \ln(k_d^{II})}{\partial(1/T)} \quad (3)$$

In previous work, it was shown that in the low-pressure limit the approximation

$$E_a = E_0 - U_{vib} - ak_BT \quad (4)$$

is valid.[6,7] Here, E_0 denotes the bond energy, U_{vib} is the vibrational energy, and a is an empirical constant ($a = 1.2$ for harmonic oscillator treatment[7]). On the basis of this approximation for E_a, integration of the Arrhenius expression yields

$$k_d^{II} = \frac{CT^{-a}\exp\left(\frac{-E_0}{k_BT}\right)}{Q_{vib}(T)} \quad (5)$$

where $Q_{vib}(T)$ is the vibrational partition function, and C is a constant. In the present work bond energies were derived by performing a weighted fit of the variation of k_d^{II} versus T (Figure 4) to eq 5. The measured rate constants were weighted as the reciprocal of k_d^{II} squared, assuming a constant fractional error in the k_d^{II} data. The resulting bond energies are listed in Table 2. Activation energies and vibrational energies at the average temperatures of the measurements are also listed in Table 2. The fit function (eq (5)) reproduces the slight curvature of the measured data (see e.g., $HSO_4^-(H_2SO_4)_3$ in Figure 4). Equation 4 is only valid in the low-pressure limit. Because the data of the larger $HSO_4^-(H_2SO_4)_x$ ($x = 2-5$) clusters were not obtained in the low-pressure limit, the fitting of the data with eq 5 yields only upper limits of the bond energies for these four clusters. This issue is discussed in detail in paper (II).

Calculations of the association rate constants for the larger clusters when the kinetics are not in the low-pressure limit confirm the fact that bond energies derived from eq 5 are just upper limits. Equilibrium constants K were calculated based on ΔS and the bond energies derived with eq 5 (Table 2), and association rate constants were calculated, using the measured decomposition rate constant, $k_{ass} = k_d^I/K$. The calculated association rate constants are $>1 \times 10^{-8}$ cm^3 s^{-1} for all clusters with more than two H_2SO_4 ligands. These unrealistic rate constants suggest that the bond energies are overestimated by eq 5. Calculating association rate constants using Su and Chesnavich's theory[25] give upper limits for the association rate constants around $1-2 \times 10^{-9}$ cm^3 molecule^{-1} s^{-1}. The bond energies derived using eq (5) can therefore only be regarded as upper limits to the true bond energies for the larger sulfuric acid clusters that have kinetics in the fall-off region.

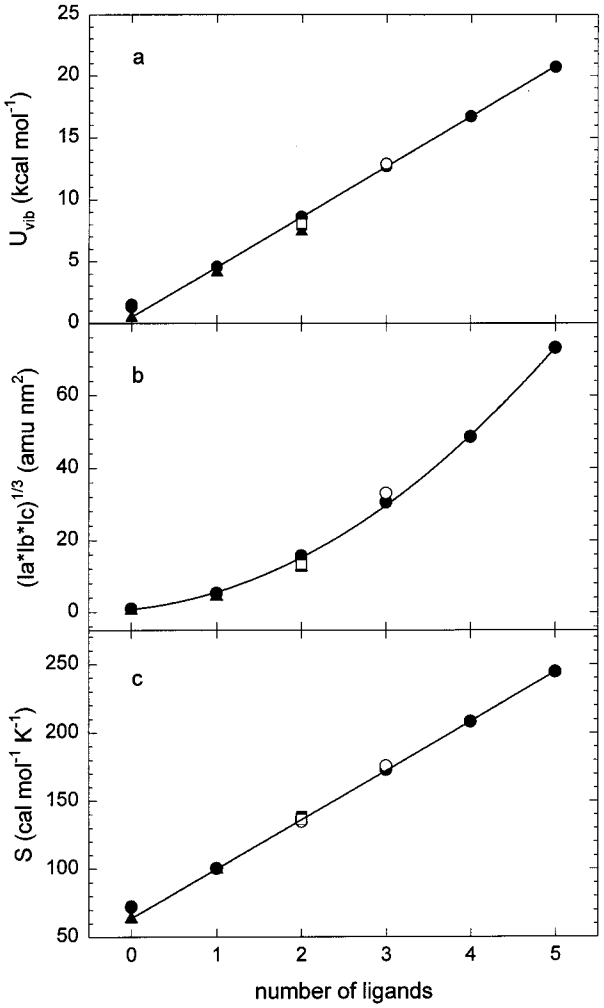

Figure 7. Thermochemical parameters of the ion clusters at 298 K as a function of the number of ligand molecules on HSO_4^-: (a) Average vibrational energies; (b) geometric mean of the moments of inertia; and (c) entropies. Symbols: solid circles = H_2SO_4 and $HSO_4^-(H_2SO_4)_x$ clusters ($x = 0-5$, most stable structures 2α and 3β); open circles = $HSO_4^-(H_2SO_4)_x$ alternate structures 2β and 3α; solid triangles = HNO_3 and $HSO_4^-(HNO_3)_y$ ($y = 1, 2$); solid square = $HSO_4^-H_2SO_4HNO_3$ structure from Figure 5(g); open square = $HSO_4^-H_2SO_4HNO_3$ structure from Figure 5(h). Regressions: (a) linear fit for $HSO_4^-(H_2SO_4)_x$ ($x = 1-4$); (b) quadratic fit for $HSO_4^-(H_2SO_4)_x$ ($x = 0-4$); and (c) linear fit for $HSO_4^-(H_2SO_4)_x$ ($x = 1-4$). For $x = 2$, 3 the more stable structures (2α and 3β) were used for the regressions.

For the remaining clusters, where the kinetics are in the low-pressure limit, the fit procedure using eq (5) yields results that are probably accurate within ±1 kcal mol^{-1}. This uncertainty was derived from the error discussion presented previously.[7] A slightly higher uncertainty of ±2 kcal mol^{-1} is assumed for the $HSO_4^-H_2SO_4$ cluster because of an increased uncertainty in the temperature measurement at the highest temperatures (~600 K). Nevertheless, it is clear that the $HSO_4^-H_2SO_4$ bond energy is exceptionally large (43 ± 2 kcal mol^{-1}), in agreement with the lower limit of 40 kcal mol^{-1} from ab initio studies of Evleth.[21] Approximate bond energies $E_{0,a.i.}$ can also be derived from the ab initio calculations. The difference between products and reactant electronic energies corrected by the differences in zero point energies are

$$E_{0,a.i.} = \sum_{\text{prod}=1,2} (E_{\text{el,prod}} + E_{\text{ZP,prod}}) - (E_{\text{el,reac}} + E_{\text{ZP,reac}}) \quad (6)$$

The ab initio bond energies $E_{0,a.i.}$ are presented in Table 2. It is interesting that these results are close (within ±3 kcal mol^{-1}) to the measured bond energies for the clusters which are in the low-pressure limit considering the fact that the ab initio calculations were not performed with a very large basis set and no basis set superposition error or electronic correlation corrections were performed. The close agreement could therefore be caused by a cancellation of errors.[12,14]

The nitric acid bond energy for association with the core ions $HSO_4^-H_2SO_4$, $HSO_4^-HNO_3$, and $NO_3^-HNO_3$ is similar, and increases slightly in the listed order (17.3, 17.7, 19.4[7] kcal mol^{-1}). In all cases, the HNO_3 forms one hydrogen bond with the core ion (Figure 5 (g), (f) and Lovejoy and Bianco[7]). The increase in bond strength going from $HSO_4^-H_2SO_4$ to $NO_3^-HNO_3$ probably reflects an increase in the availability of the charge. HSO_4^- is a weaker base than NO_3^-, and HSO_4^- bonds more strongly to H_2SO_4 than HNO_3. The bond energy trend is consistent with the general trends highlighted by Caldwell and Kebarle[26] for the hydrogen bond energies of bihalide ions YHX^-. They note that the YHX^- clusters are more stable for more acidic YH and more basic X^-. Comparison of the bond energies of $HSO_4^-HNO_3$ and $NO_3^-HNO_3$ shows that HNO_3 bonds slightly stronger to HSO_4^- (27.2 vs 26.0 kcal mol^{-1}), even though NO_3^- is a stronger base than HSO_4^-. This is probably because HNO_3 is able to form two hydrogen bonds to HSO_4^-, but only one with NO_3^-. A detailed comparison of the $HSO_4^-(H_2SO_4)_x(HNO_3)_y$ bond energies with the thermochemical data reported by Arnold and co-workers[8] is given in paper (II).

Summary

Measurements of the temperature and pressure dependence for the dissociation of sulfuric and nitric acid ion clusters in an ion trap were presented. Ab initio calculations yielded information on the structures, vibrational frequencies, vibrational energies, moments of inertia, and entropies of these clusters. Bond energies for $HSO_4^-(H_2SO_4)_x$ ($x = 1-5$), $HSO_4^-(HNO_3)_y$ ($y = 1, 2$) and $HSO_4^-H_2SO_4HNO_3$ were derived from the temperature dependence of the second-order decomposition rate coefficients based on the relationship $E_0 = E_a + U_{vib} + ak_BT$. It was shown that this relationship yields only an upper limit of the bond energies for the larger ion clusters ($HSO_4^-(H_2SO_4)_x$ for $x \geq 2$) for which the kinetics are in the fall-off region. However, fitting the data with a master equation model presented in the accompanying paper shows that accurate bond energies can be obtained from this data set. Bond energies derived from the ab initio calculations are close to the measured bond energies. The bond energy of the triply hydrogen bonded $HSO_4^-H_2SO_4$ cluster is larger than 40 kcal mol^{-1}.

The derived bond energies are essential for the molecular modeling of ion-induced nucleation processes. In this paper, pure sulfuric acid and sulfuric acid/nitric acid cluster ions were studied. Future studies will focus on other systems of atmospheric importance, such as the binary systems H_2SO_4/H_2O and H_2SO_4/NH_3.

Acknowledgment. We thank the NOAA Forecast Systems Lab for a generous allotment of computer time on the JET computer cluster facility. We thank Dr. Roberto Bianco of the University of Colorado at Boulder for providing us with optimized semiempirical structures of the $HSO_4^-(H_2SO_4)_x$, $x = 1-5$, complexes from which the current optimized HF/6-31+G(d) structures and vibrational frequencies were derived. We acknowledge helpful discussion with D. Hanson. We thank an anonymous reviewer for motivating the current bond energy fitting routine. This work was performed while J.C. held a National Research Council Research Associateship Award at the NOAA Aeronomy Lab. The work was supported in part by NOAA's Climate and Global Change Program.

Supporting Information Available: Structures, moments of inertia and vibrational frequencies for cluster ions and ligands calculated at the HF/6-31+G(d) level. This material is available free of charge via the Internet at http://pubs.acs.org.

References and Notes

(1) Arnold, F.; Henschen, G. *Nature* **1978**, *257*, 521. Arnold, F.; Viggiano, A. A.; Schlager, H. *Nature* **1982**, *297*, 371. Eisele, F. L. *J. Geophys. Res.* **1989**, *94*, 2183. Viggiano, A. A.; Arnold, F. *Handbook of Atmospheric Electrodynamics*; Volland, H., Ed.; CRC Press: London, **1995**, *1*, 1. Arijs, E. *Planet Space Sci.* **1992**, *40*, 255. Beig, G.; Brasseur, G. P. *J. Geophys. Res.* **2000**, *105*, 22 671.

(2) Arnold, F. *Nature* **1980**, *284*, 610. Arnold, F.; Viggiano, A. A.; Schlager, H. *Nature* **1982**, *297*, 371. Raes, F.; Janssens, A.; van Dingenen, R. *J. Aeros. Sci.* **1986**, *17*, 466. Turco, R. P.; Zhao, X.-J.; Yu, F. *Geophys. Res. Lett.* **1997**, *24*, 1927. Yu, F.; Turco, R. P. *Geophys. Res. Lett.* **2000**, *27*, 883.

(3) Yu F.; Turco, R. P.; Kärcher, B.; Schröder, F. P. *Geophys. Res. Lett.* **1998**, *25*, 3839. Arnold, F.; Curtius, J.; Sierau, B.; Bürger, V.; Busen, R.; Schumann, U. *Geophys. Res. Lett.* **1999**, *26*, 1577.

(4) Viggiano, A. A.; Perry, R. A.; Albritton, D. L.; Ferguson, E. E.; Fehsenfeld, F. C. *J. Geophys. Res.* **1982**, *87*, 7340. Viggiano, A. A.; Seeley, J. V.; Mundis, P. L.; Williamson, J. S.; Morris, R. A. *J. Phys. Chem.* **1997**, *101*, 8275.

(5) Weber, R. J.; Marti, J. J.; McMurry, P. H.; Eisele, F. L.; Tanner, D. J.; Jefferson, J. *J. Geophys. Res.* **1997**, *102*, 4375. Weber, R. J.; et al. *J. Geophys. Res.* **1998**, *103*, 16 385. Clarke, A. D. *Science* **1998**, *282*, 89.

(6) Troe, J. *J. Chem. Phys.* **1977**, *66*, 4745. For a comprehensive introduction see: Smith, I. W. M. *Modern Gas Kinetics − Theory, Experiment and Application*; Pilling, M. J., Smith, I. W. M., Eds.; Blackwell Scientific Publications: Oxford, 1987; pp 99−134.

(7) Lovejoy, E. R.; Bianco, R. *J. Phys. Chem. A* **2000**, *104*, 10 280.

(8) Arnold, F.; Viggiano, A. A.; Schlager, H. *Nature* **1982**, *297*, 371. Arnold, F.; Qiu, S. *Planet Space Sci.* **1984**, *32*, 169. Qui S.; Arnold, F. *Chinese Space Physics* **1985**, *4*, 293.

(9) Lovejoy, E. R.; Wilson, R. *J. Phys. Chem. A* **1998**, *102*, 2309.

(10) Franzen, J. *Int. J. Mass Spectrom. Ion Processes* **1993**, *125*, 165.

(11) Asano, K. G.; Goeringer, D. E.; McLuckey, S. A. *Int. J. Mass Spectrom.* **1999**, *185/186/187*, 207.

(12) Davidson, E. R.; Feller, D. *Chem. Rev.* **1986**, *86*, 681.

(13) Simon, S.; Duran, M.; Dannenberg, J. J. *J. Phys. Chem. A* **1999**, *103*, 1640.

(14) Head-Gordon, M. *J. Phys. Chem.* **1996**, *100*, 13 213.

(15) Raghavachari, K.; Anderson, J. B. *J. Phys. Chem.* **1996**, *100*, 12 960.

(16) Scott, A. P.; Radom, L. *J. Phys. Chem.* **1996**, *100*, 16 502. For consistency, the same scaling factor as in Lovejoy and Bianco[7] was used. Scott and Radom recommend slightly different scaling factors between 0.8945 and 0.9153 for the HF/6-31+G(d) level of theory depending on the property calculated. These authors note that the scaling factor decreases

slightly with increasing temperature. A sensitivity study presented in paper (II), which varies the scaling factor, shows that the bond energies are insensitive to the exact value of the scaling factor within the range of 0.90 ± 0.02.

(17) Schmidt, M. W.; Baldridge, K. K.; Boatz, J. A.; Elbert, S. T.; Gordon, M. S.; Jensen, J. H.; Koseki, S.; Matsunaga, N.; Nguyen, K. A.; Su, S.; Windus, T. L.; Dupuis, M.; Montgomery, J. A. *J. Comput. Chem.* **1993**, *14*, 1347.

(18) Schaftenaar, G.; Noordik, J. H. *J. Comput.-Aided Mol. Design* **2000**, *14*, 123.

(19) Kuczkowski, R. L.; Suenram, R. D.; Lovas, F. J. *J. Am. Chem. Soc.* **1981**, *103*, 2561.

(20) Re, S.; Osamura, Y.; Morokuma, K. *J. Chem. Phys. A* **1999**, *103*, 3535.

(21) Evleth, E. M. *J. Mol. Struct. (Thermochem)* **1994**, *307*, 179−185.

(22) Chase, M. W., Jr.; Davies, C. A.; Downey, J. R., Jr.; Frurip, D. J.; McDonald, R. A.; Syverud, A. N.; JANAF Thermochemical Tables. *J. Phys. Chem. Ref. Data Suppl. 1* **1985**, 14.

(23) Larson, J. L.; Largent, A.; Tao, F.-M. *J. Phys. Chem. A* **1999**, *103*, 6786.

(24) Xantheas, S. S.; Dunning, T. H., Jr. *J. Chem. Phys.* **1993**, *99*, 8774.

(25) Su, T.; Chesnavich, W. J. *J. Chem. Phys.* **1982**, *76*, 5183.

(26) Caldwell, G.; Kebarle, P. *Can. J. Chem.* **1985**, *63*, 1399.

(27) Lovejoy, E. R.; Curtius, J. *J. Phys. Chem. A* **2001**, *105*, 10874.